Steel and Composite Structures, Vol. 5, No. 6 (2005) 421-441
DOI: http://dx.doi.org/10.12989/scs.2005.5.6.421

Numerical predictions of the time-dependent temperature field for the 7th Cardington compartment fire test

António M. G. Lopes†

Department of Mechanical Engineering, University of Coimbra,
Polo II - Pinhal de Marrocos, 3030-290 Coimbra, Portugal

Gilberto C. Vaz‡

Department of Mechanical Engineering, ISEC, Polytechnic Institute of Coimbra,
Rua Pedro Nunes, 3030-199 Coimbra, Portugal

Aldina Santiago‡†

Department of Civil Engineering, University of Coimbra,
Polo II - Pinhal de Marrocos, 3030-290 Coimbra, Portugal

(Received December 9, 2004, Accepted May 23, 2005)

Abstract. The present work reports on a numerical simulation of a compartment fire. The fire was modeled using a simplified approach, where combustion is simulated as a volumetric heat release. Computations were performed with the commercial code CFX 5.6. Radiation was modeled with a differential approximation (P1 model), while turbulence effects upon the mean gas flow were dealt with a SST turbulence model. Simulations were carried out using a transient approach, starting at the onset of ignition. Results are provided for the temperature field time evolution, thus allowing a direct comparison with the analytical and experimental data. The high spatial resolution available for the results proved to be of great utility for a more detailed analysis of the thermal impact on the steel structure.

Key words: compartment fire; experimental fire tests; fire safety engineering; numerical simulation; temperature distribution.

1. Introduction

Global structural behaviour of steel and composite structures under the action of a fire is a subject of the utmost importance in what concerns security issues in buildings. How a fire may impact on the building structure is a subject that can only be addressed with the knowledge of the response of the structure to high temperatures and how temperatures develop as consequence of a fire occurrence.

†Assistant Professor, Corresponding author, E-mail: antonio.gameiro@dem.uc.pt
‡Assistant Professor, E-mail: gcvaz@mail.isec.pt
‡†Research Assistant, E-mail: aldina@dec.uc.pt

The calculations performed to assess the structural fire safety are organized in three steps: 1st - evaluation of the gas temperature on the fire compartment; 2nd - calculation of the temperature on the structure and 3rd - calculation of the mechanical behaviour of the structure exposed to fire. The last aspect will not be dealt with detail in this paper, generic references being available (Wang 2002, Vila Real 2003). Additionally, reference is also made to other two papers that address these issues in more detail in the context of the 7th Cardington fire test (Wald *et al.* 2004, Simões da Silva *et al.* 2004).

Concerning the gas temperature on the fire compartment, a distinction is made in the prEN1991-1-2:2002 between nominal fire curves and natural fire models. Nominal fires are conventional fires which can be expressed by a simple formula and which are assumed to be identical whatever is the size or the design of the building. Theses curves do not reproduce a real fire; however they are used to check if an element has the required level of fire resistance to fulfil the normative requirements.

Natural fire models can be used for evaluating the dynamics of a real fire. They are classified from the simplest calculation models like Parametric Temperature-Time Curves, Zone Models, to more advanced models such as those based on Computational Fluid Dynamics - CFD (Cadorin 2003). These natural fire models take into account the main parameters which influence the growth and development of fire: size of the compartment, fire load, ventilation conditions, etc.

Parametric temperature-time curves have the form of simple equations based on theoretical developments and experimental correlations. They refer to a fully developed fire that creates the same temperature throughout the fire compartment (prEN1991-1-2:2002). Zone models are developed to predict the temperature evolution of the gases within the compartment during the fire. This type of models considers the compartment as divided in different zones characterized by a uniform temperature distribution at every given time (Cadorin *et al.* 2003a,b). Single-zone models are usually adopted to simulate fully developed fires, while two-zone models are intended to be applied to localised fires or during the pre-flashover phase. Computational Fluid Dynamic models are the most physically complete models to simulate compartment fires (eg. Markatos *et al.* 1982, 1984, Hoffmann *et al.* 1988, 1989, Cox 2001). They are based on the fundamental conservation laws for mass, momentum and energy, and the corresponding equations are usually solved through the finite volume method. In spite of the ever-growing computational power, both in terms of speed and memory capacity, direct numerical simulation is still not feasible for most practical problems, due to the high spatial and temporal resolution required for direct simulation of the fluctuations due to turbulence. Thus, a turbulence model is used for simulating the effect of fluctuation upon the mean flow, both in terms of velocity and temperature fields.

Several CFD commercial codes are presently available, such as SOFIE, developed at the Cranfield University (Rubini 2000), SMARTFire, developed at the University of Greenwich (Ewer *et al.* 1999) and FDS, developed at NIST (McGrattan *et al.* 2000). In the present work, the CFD model CFX 5.6 (from ANSYS) is applied for the simulation of the temperature field time evolution during the 7th Cardington fire test. This fire test was carried out under the scope of the collaborative research project "Tensile membrane action and robustness of structural steel joints under natural fire" (EC FP5 HPRI-CV 5535), involving the Czech Technical University (Czech Republic), the University of Coimbra (Portugal), the University of Bratislava (Slovak Republic) and the Building Research Establishment (England). The main goal of this test fire was to investigate the global structural behaviour of a compartment in a steel frame building. During the fire test, time-temperature in the fire compartment and in beams, columns, connections and composite slab were recorded. The corresponding distribution of internal forces and deformations of the main structural members were also evaluated (Wald *et al.* 2005).

2. The numerical model

Numerical simulations were performed with the commercial code CFX 5.6. It is a general-purpose code for fluid dynamics and heat transfer modelling. It employs a finite-volume formulation in unstructured meshes, thus allowing a good geometrical flexibility.

2.1. Governing equations

Conservation of momentum is described by the Navier-Stokes equations, which time dependent formulation is:

$$\frac{\partial(\rho u_i)}{\partial t} + \frac{\partial}{\partial x_j}(\rho u_j) = -\frac{\partial p}{\partial x_i} + \frac{\partial \tau_{ij}}{\partial x_j} - \frac{2}{3}\frac{\partial(\rho k)}{\partial x_i} + S_i \tag{1}$$

where τ_{ij} represents the stress tensor, k is the turbulence kinetic energy, ρ is the fluid density and S_i is the momentum source due to temperature differences in the fluid:

$$S_i = (\rho - \rho_{ref})g_i \tag{2}$$

The continuity equation formulates the principle of mass conservation:

$$\frac{\partial \rho}{\partial t} + \frac{\partial}{\partial x_j}(\rho u_j) = 0 \tag{3}$$

The energy equation is:

$$\frac{\partial \rho h}{\partial t} - \frac{\partial p}{\partial t} + \vec{\nabla}(\rho \vec{V} h) = \vec{\nabla}(\lambda \vec{\nabla} T) + S_E \tag{4}$$

where the specific enthalpy is given by $dh = c_p\, dT$ and S_E is the energy source term.

For modeling the entire radiation phenomena, a transport equation must be solved for the radiative heat transfer in fluid and gas media.

According to CFX documentation, the spectral radiative transfer equation can be written as

$$\frac{dI_\nu(\mathbf{r}, \mathbf{s})}{ds} = -(K_{a\nu} + K_{s\nu})I_\nu(\mathbf{r}, \mathbf{s}) + K_a I_b(\nu, T) + \frac{K_{s\nu}}{4\pi}\int_{4\pi} dI_\nu(\mathbf{r}, \mathbf{s}')\, \Phi(\mathbf{s} \cdot \mathbf{s}')d\Omega' + S \tag{5}$$

where ν - frequency, **r**- position vector, **s**- direction vector, s - path length, K_a - absorption coefficient, K_s - scattering coefficient, I_b - blackbody emission intensity, I_ν - spectral radiation intensity, T - local absolute temperature, Ω - solid angle, Φ - in-scattering phase function, S - radiation intensity source term.

Eq. (5) is a first order integro-differential equation for I_ν in a fixed direction. To solve this equation within the domain, a boundary condition for I_ν is required. In this study, the walls are considered as diffusely emitting and reflecting opaque boundaries and the openings are considered fully transparent boundaries.

Due to the dependence on 3 spatial coordinates and 2 local direction coordinates, s and ν, the formal solution of the radiative transfer Eq. (5) is very time consuming, requiring the use of approximate models for the directional and spectral dependencies. For the directional approximation, the P1 model is adopted (see Raithby 1991, for details). This model, also known as the Gibb's model or Spherical

Harmonics model, assumes that the radiation intensity is isotropic or direction independent at a given location in space. The spectral radiative heat flux in the diffusion limit for an emitting, absorbing, and linearly scattering medium, can be computed as:

$$q_{rv} = -\frac{1}{3(K_{av}-K_{sv})-AK_{sv}}\nabla G_v \tag{6}$$

where A is the linear anisotropy coefficient and G_ν is the spectral incident radiation. Then, the equation for the spectral incident radiation is:

$$-\nabla.\left(\frac{1}{3(K_{av}-K_{sv})-AK_{sv}}\nabla G_v\right) = K_{av}(E_{bv}-G_v) \tag{7}$$

where $E_{b\nu}$ is the spectral blackbody emission.

For the wall treatment, assuming that the radiation intensity arriving at and leaving a wall is directionally independent, the boundary condition for (7) at the wall is:

$$\mathbf{n}\cdot\mathbf{q}_{rv} = -\frac{1}{3(K_{av}-K_{sv})-AK_{sv}}\frac{\partial G_v}{\partial n^+} = \frac{\varepsilon_v}{2(2-\varepsilon_v)}[E_{bv}-G_v]\big|_w \tag{8}$$

where $\mathbf{n}$ is the unit vector outward normal to the wall, n^+ is a distance coordinate in the same direction, ε_v is the spectral emissivity and w represents the value at the wall.

For the spectral approximation, the gray model is adopted. This model assumes that all radiation quantities are nearly uniform throughout the spectrum. Then, the dependency of Eq. (5) on frequency can be dropped. The scattering model adopted is the isotropic model, assuming that in-scattering is uniform in all directions.

For closing the problem, a state equation is necessary for describing the relation between temperature, pressure and density. In the present case, this is achieved considering the gases inside the compartment to behave as a perfect gas with constant specific heat capacity c_p.

Turbulence effects upon the mean flow were simulated with the SST model (Menter 1993, 1994), which is a weighted blending of the k-ω model (Wilcox 1993) and the standard k-ε of Launder and Spalding (1974), according to the boundary layer region where the solution takes place. The equations are:

$$\frac{\partial}{\partial x_i}(\rho u_i k) = \frac{\partial}{\partial x_i}\left[\left(\mu+\frac{\mu_t}{\sigma_{k3}}\right)\frac{\partial k}{\partial x_i}\right] + P_k - \beta'\rho k\omega \tag{9}$$

$$\frac{\partial}{\partial x_i}(\rho u_i \omega) = \frac{\partial}{\partial x_i}\left[\left(\mu+\frac{\mu_t}{\sigma_{\omega 3}}\right)\frac{\partial \omega}{\partial x_i}\right] + \alpha_3\frac{\omega}{k}P_k - \beta_3\rho\omega^2 + (1-F_1)2\rho\sigma_{\omega 2}\frac{1}{\omega}\nabla k\nabla\omega \tag{10}$$

where the index 3 coefficients are obtained as a linear combination of the index 1 (corresponding to the k-ε model) and the index 2 (corresponding to the k-ω model) coefficients, as defined next:

$$\beta' = 0.09 \quad \alpha_1 = 5/9 \quad \beta_1 = 3/40 \quad \sigma_{k1} = 2 \quad \sigma_{\omega 1} = 2$$
$$\alpha_2 = 0.44 \quad \beta_2 = 0.0828 \quad \sigma_{k2} = 1 \quad \sigma_{\omega 2} = 0.856$$

As a means of limiting the turbulence kinetic energy production in stagnation regions, its term is computed as follows:

$$\tilde{P}_k = \min(P_k, 10\varepsilon) \tag{11}$$

The weighting factor F_1 is obtained with the following equation:

$$F_1 = \tanh\left(\min\left(\max\left(\frac{\sqrt{k}}{\beta'\omega y}, \frac{500\nu}{y^2\omega}\right), \frac{4\rho\sigma_{\omega 2}k}{CD_{k\omega}y^2}\right)\right)^4 \tag{12}$$

$$CD_{k\omega} = \max\left(2\rho\sigma_{\omega 2}\frac{1}{\omega}\nabla k\nabla\omega, le-10\right) \tag{13}$$

Modelling of the shear stress transport is accomplished with a limiting factor in the formulation of the turbulence viscosity:

$$\upsilon_t = \frac{a_1 k}{\max(a_1\omega, SF_2)} \tag{14}$$

where:

$$F_2 = \tanh\left(\max\left(\frac{2\sqrt{k}}{\beta'\omega y}, \frac{500\nu}{y^2\omega}\right)\right)^2 \tag{15}$$

and S quantifies the fluid deformation rate (cf. Menter 1993, 1994, for details).

2.2. Grid characteristics

The unstructured grid of CFX 5.6 is based on triangular element discretization for the generation of surface grids. The volume grid is constituted by tetrahedral elements, produced through the Advancing Font and Inflation method. Near surfaces, an inflation layer made of prismatic and pyramidal elements, may be optionally produced, in order to better resolve boundary gradients. Global length, surface maximum and minimum length and inflation height are some of the grid control parameters used in the grid generation module of CFX 5.6. They control, respectively, the grid size inside the domain, far from the boundaries; the maximum and minimum allowed grid size in the surface; and the thickness of the prismatic elements layer near the surface. Good spatial resolution near the walls is particularly important in problems involving heat transfer, as a fundamental requirement for a correct modelling of the energy fluxes between the fluid and the solid surfaces.

3. Statement of the physical problem

3.1. Test building and the fire compartment

The steel building structure was built inside a former airship hangar located at Cardington, Bedfordshire, UK, in the early 90's. The test building is a steel framed construction, using concrete slabs supported by a steel decking and in composite action with the steel beams. It has eight storeys (33 m) and is five bays wide (5×9 m) by three bays deep (6+9+6=21 m) in plan. Construction details of the building structure are given in Bravery (1993). The compartment was situated in the middle of the

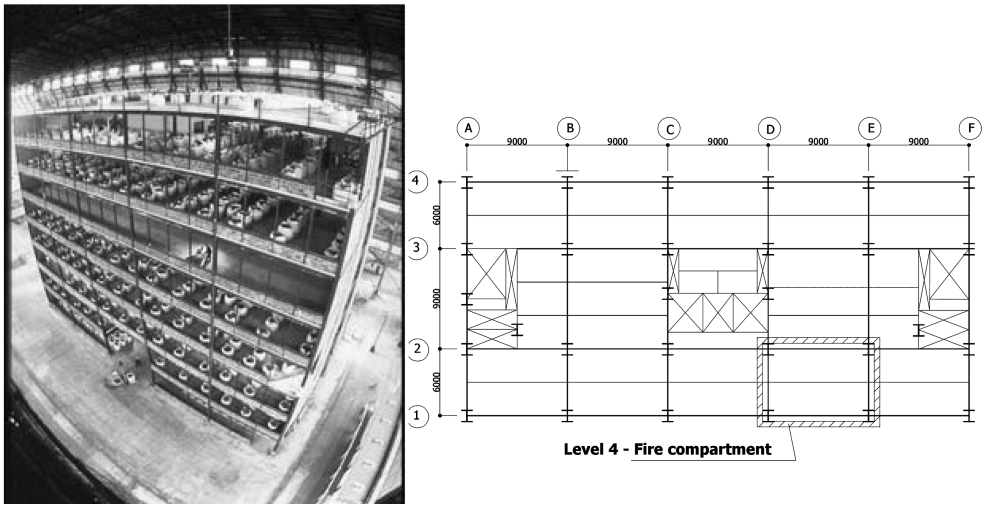

Fig. 1 Cardington fire test: a) The eight storey steel structure; b) The fire compartment (Wald *et al.* 2005)

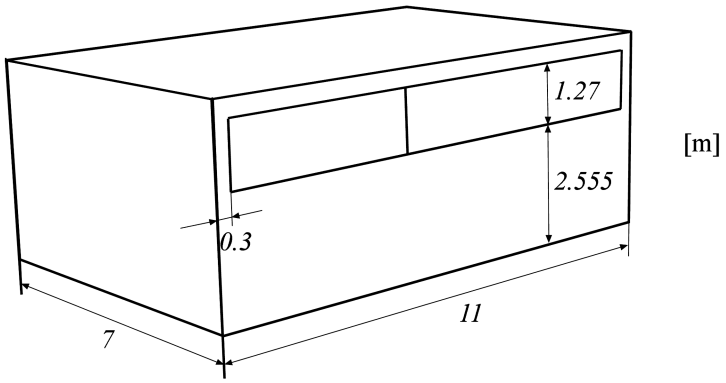

Fig. 2 Schematic representation of the fire compartment

building enclosing a plan area of 11×7 m^2, on the 4th floor, with a ceiling height of 4.185 m and a ventilation opening with 10.4×1.27 m^2 (Fig. 1). The walls are composed of three layers of plasterboard plates (15 mm + 12.5 mm + 15 mm) with thermal conductivity in the range k = 0.19-0.24 W/mK. Ceiling and floor are made of concrete (k = 0.7 W/mK) with about 0.11 m thickness. The columns, external joints and connected beam (approximately 1.0 m from the joint) were heavily fire protected to prevent global structural instability. The material protection used was 15 mm of Cafco300 vermiculite-cement spray, with thermal conductivity k = 0.078 W/mK (Wald *et al*. 2005). The computer model of the fire compartment is shown in Fig. 2.

The fire load was provided by a geometrically regular arrangement of 32 wooden cribs made of 10 piles of wooden sticks (as shown in Figs. 3 and 4), representing a fuel load of 40 kg/m^2 (of floor area), as shown in Fig. 3. Each pile was approximately 0.5 m high.

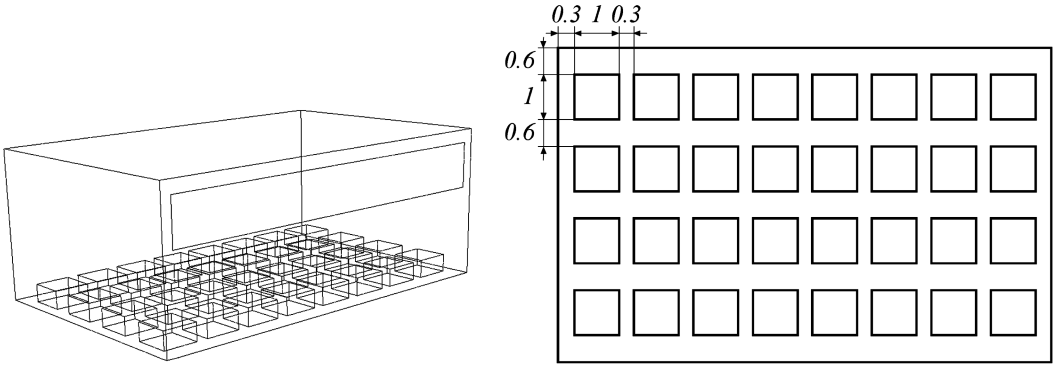

Fig 3. Schematic representation of wood cribs distribution

Fig 4 View of the wood cribs (Wald *et al.* 2005)

4. Physical modelling and numerical approach

4.1. Rate of heat release

Detailed simulation of the pyrolisis processes within the fuel was not undertaken. Instead, a simplified approach was adopted, where the fire is modelled as a heat source in the volumetric region initially occupied by the wood.

The total energy available is:

$$E_{tot} = \eta H q_{f,m} A_f \tag{16}$$

where $\eta = 0.875$ is the combustion efficiency, $H = 16$ MJ/kg is the wood heat content, $q_{f,m} = 40$ kg/m^2 is the fuel load density and $A_f = 77$ m^2 is the compartment floor area. Substitution of the corresponding values in the previous equation gives a total of 4.312×10^{10}J of available energy.

Dependence of rate of heat release (RHR) with time is one of the most important parameters for this type of simulation, and probably the most difficult to estimate. Unfortunately, during the experimental

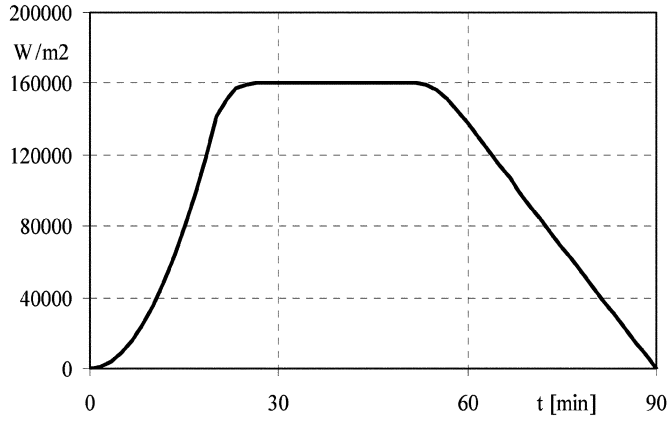

Fig. 5 NFSC design curve for heat release as a function of time. Curve 1

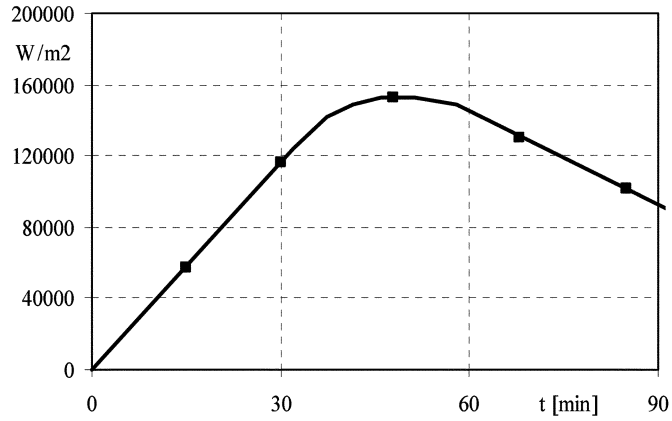

Fig. 6 RHR curve based on NFSC19 experiment. Curve 2

tests, no data was measured for the rate of wood mass loss as a function of time. An estimation of the RHR had then to be made. For that, two curves described by Cadorin (2003) were taken for testing. The first curve, which seems to be the less realistic, is adopted by the NFSC (Natural Fire Safety Concept) and it is also described by the prEN1991-1-2:2002, Annex E, for design fires. The corresponding rate of heat release as a function of time is depicted in Fig. 5. During the fire growth phase, RHR is proportional to t^2. After this initial stage, RHR is constant in time (steady state phase), and then there is a linear decrease with time. The decreasing phase is assumed to start when 70% of the total fuel is consumed. RHR was computed so that its integral over the total time approaches the total energy available. For this case, it was assumed that 90 minutes after fire ignition, all the available energy had been released.

The second curve is also presented by Cadorin (2003). It pertains data obtained in a laboratory fire, referred as NFSC19 in the NFSC database. In the present work, the peak heat release rate of the original curve was made to coincide with the instant of maximum measured temperature and it was ensured that the curve integral approximates the total energy available in the compartment. The resulting RHR curve is depicted in Fig. 6. As may be seen, in this case, some energy was yet to be released after the 90 minutes of simulation. The dots in this curve indicate time instants where numerical and experimental temperature data was compared.

4.2. Boundary conditions

For the present calculations, the delay in thermal response of the walls and ceiling due to thermal inertia was not simulated. In fact, the referred transient behaviour leads to a delay on both heating and cooling times for the solid boundaries and this is a function of the solid material thermal characteristics, their geometric configuration and total mass involved in the process. In the present case, the solid boundaries were relatively thin, and thus, the error due to the approximation adopted is relatively small. The heat flux at the wall is computed assuming a linear temperature profile within the solid, taking the well known heat conduction equation, as follows:

$$\dot{q}_w = \frac{T_{wi} - T_{wo}}{\sum \delta_j / k_j} \tag{17}$$

The variables T_{wi} and T_{wo} are the internal and external wall temperature, respectively, and δ_i and k_i are the thickness and thermal conductivity of the material(s) composing each layer in the walls and ceiling of the compartment. According to the measurements, the external ambient temperature during the experiments was, approximately, 20°C.

For radiation computation, gases inside the compartment are assumed to have an average absorption coefficient of 0.3 m^{-1}, which is a reasonable assumption based on experimental data (Thomas 1971). All solid boundaries are opaque, with an emissivity of 0.9 and a diffuse fraction of 0.9. For the opening, a static relative pressure of 0 Pa was assigned.

4.3. Grid and time step dependence tests

Due to the symmetric character of both the geometry and boundary conditions, the problem was solved in half the domain, with symmetry conditions imposed at the middle plane. For better resolving the velocity gradients and energy fluxes at the walls, a grid refinement with prismatic elements was imposed at all the solid boundaries, with the first grid point 3 mm away from the solid surfaces. Three different grids, A, B and C were tested, using 61000, 117000 and 220000 nodes, respectively. For these

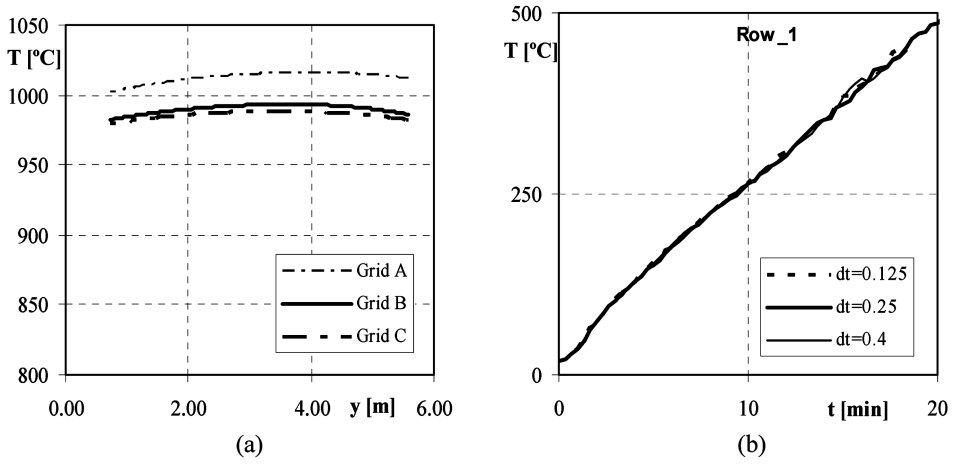

Fig. 7 Grid and time-step dependence tests

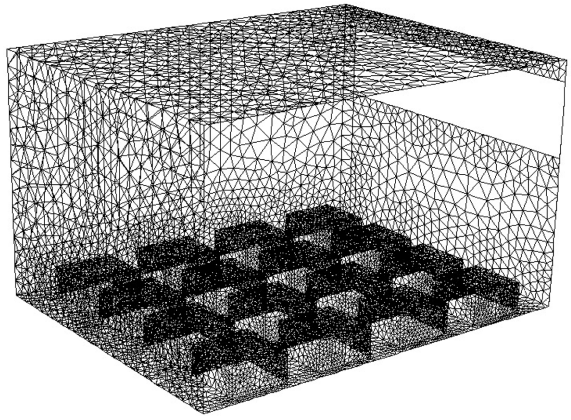

Fig. 8 Non-structured grid employed in the simulations. Only half the domain is represented.

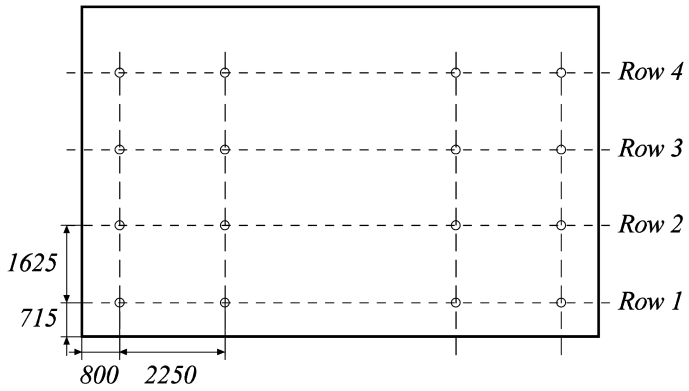

Fig. 9 Location of the thermocouples position for gas temperature measurement. Compartment opening is at the bottom.

tests, a steady state condition was adopted, with a heat release of 93000 W/m^2. The temperature distribution from the opening to the back of the compartment, at a height of 300 mm from the ceiling, at the symmetry plane, is depicted in Fig 7(a). Since the results obtained using grids B and C are not significantly different, grid B, depicted in Fig. 8, was select for the full numerical computations.

The influence of the time step was tested with the values 0.4 s, 0.25 s and 0.125 s. Fig. 7(b) shows the results for the average temperature along row 1 (cf. Fig. 9) at the early stages of fire development, using the heat release curve 2. It may be seen that there are no significant differences between the several curves. In order to ensure a good stability, the 0.25 s time-step was selected.

5. Results

Numerical simulations were carried out using a transient approach, setting as initial conditions gas temperature at 20°C and 0 m/s for gas velocity. Total simulation time was 90 min, thus corresponding to a total of 21600 time steps. For convergence criteria, the residuals of all equations were kept below 10^{-4}.

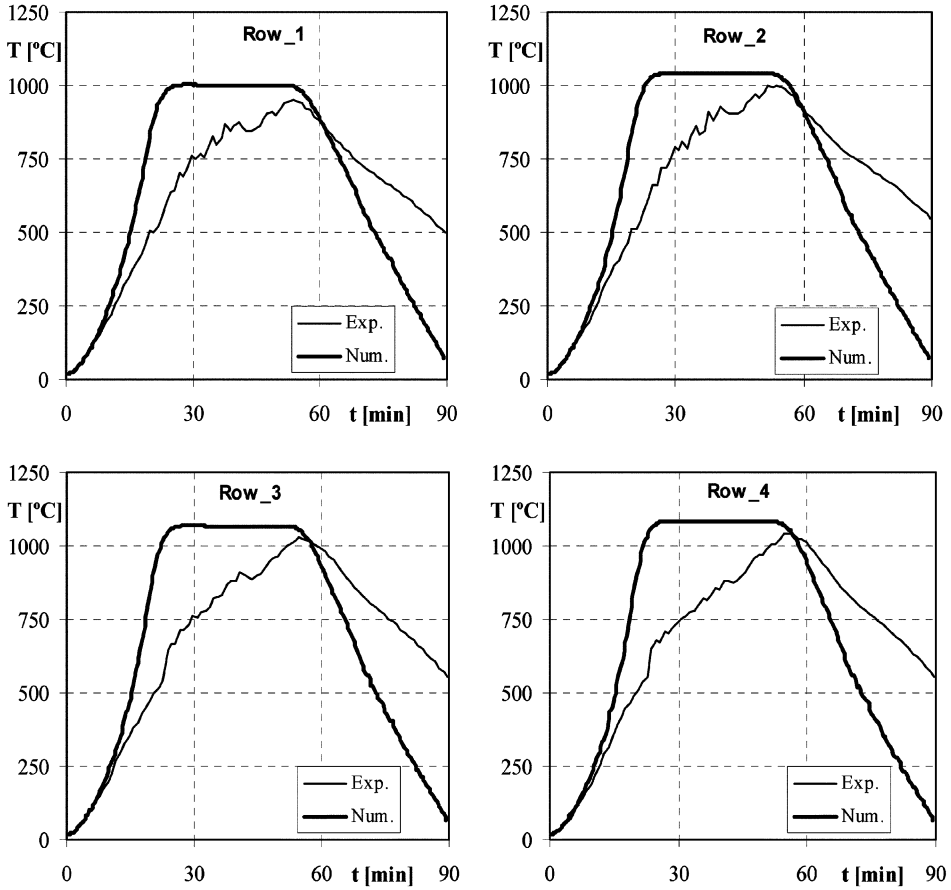

Fig. 10 Comparison between simulated and measured temperatures. RHR curve 1

Total computation time was approximately 12 full days of CPU time, in a Dual-Xeon at 2.8 GHz personal computer with 2.0 MB of RAM.

During the experimental fire, temperatures were recorded in the compartment with several thermocouples, positioned 300 mm from the ceiling, at the locations represented by small circles in Fig. 9. Comparison of numerical and experimental data for temperature versus time is made for the average values along each row, as defined in this figure. The results obtained using RHR curve 1 as input (cf. Fig. 5) are shown in Fig. 10. As may be observed, the time evolution of the predicted temperatures closely follows the overall trend of the heat release rate, presenting significant differences with respect to the experimental temperature data, with exception of the initial stages of fire growth. The time delay effect due to the thermal inertia of the walls and ceiling, which was not taken into account in the simulations, is not believed, by no means, to be large enough to explain this difference. As a matter of fact, this relatively poor comparison could be somehow anticipated. The RHR plateau during the maximum burning rate is mostly typical of ventilation controlled fires, which occur when the ventilation openings are not large enough to supply all the oxygen flowrate that the fire would consume. In this case, the burning rate becomes dependent on the availability of oxygen (the fire is said to be "ventilation controlled") and exhibits a typical plateau on RHR versus time, as the one present in curve 1.

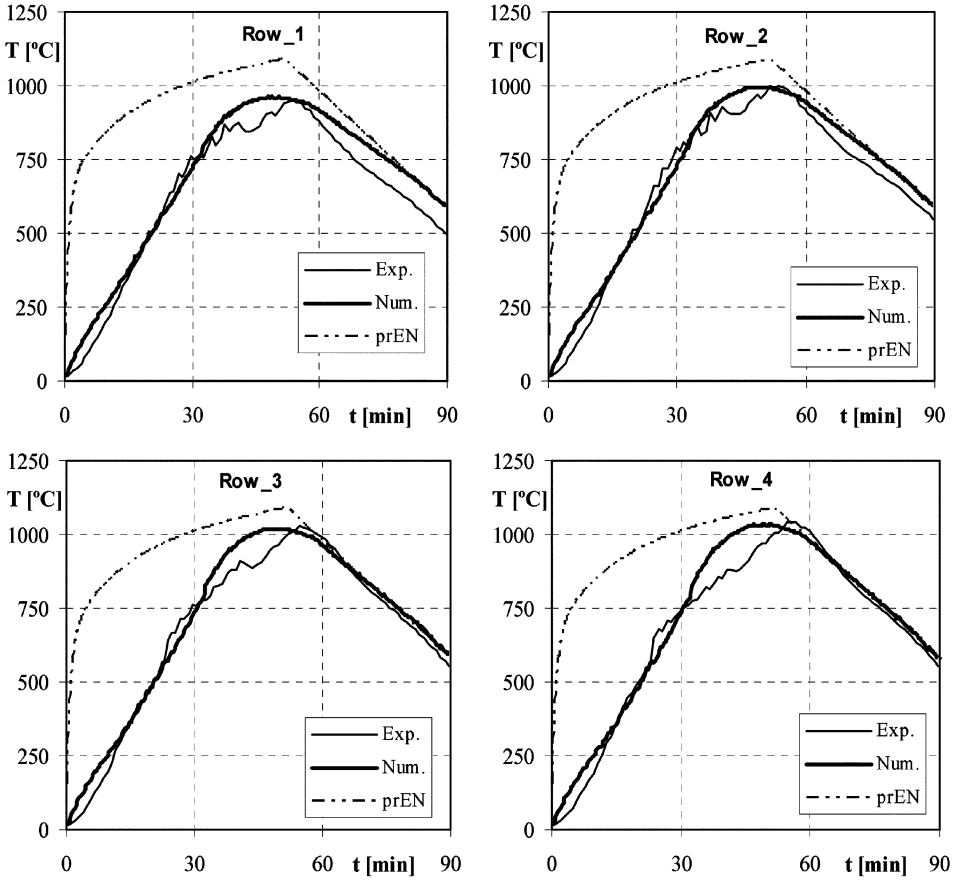

Fig. 11 Comparison between numerical and experimental temperature data. RHR curve 2

On the other hand, if ventilation is enough, the fire is controlled by the available amount of fuel. In this case, the fire is said to be "fuel controlled". Although not strictly rigid, a criteria proposed by Harmathy (1978) allows fire classification in terms of fuel- or ventilation-controlled as follows: a ventilation factor is defined based on the opening dimensions:

$$V_f = A_w h_w^{1/2} \tag{18}$$

where A_w and h_w are the opening area and height, respectively. The distinction between ventilation- and fuel-controlled fires is established as follows:

$$V_{ft} = \frac{\rho g^{1/2} V_f}{A_{fi}} < 0.235 \quad \text{for ventilation control} \tag{19}$$

$$V_{ft} = \frac{\rho g^{1/2} V_f}{A_{fi}} > 0.290 \quad \text{for fuel control} \tag{20}$$

where ρ is the gas density and A_{fi} is the horizontal fire area, which, in this case, is approximately equal to the compartment floor area. For the case under study, $V_{fi} = 0.7$, leading us to conclude that the fire is clearly fuel-controlled. Oxygen supply is not limiting the burning rate and thus, it is not expected that the heat release rate presents such a plateau as the one prescribed by the design curve 1.

One may, now, foresee that results obtained with RHR curve 2 should be better, as this curve presents, in terms of overall trend, a closer similarity with the temperature development within the compartment. The corresponding results are shown in Fig. 11, where the temperature predicted by the parametric curve given in prEN 1991-1-2:2002 (see Annex A) and experimental data are also depicted. We may

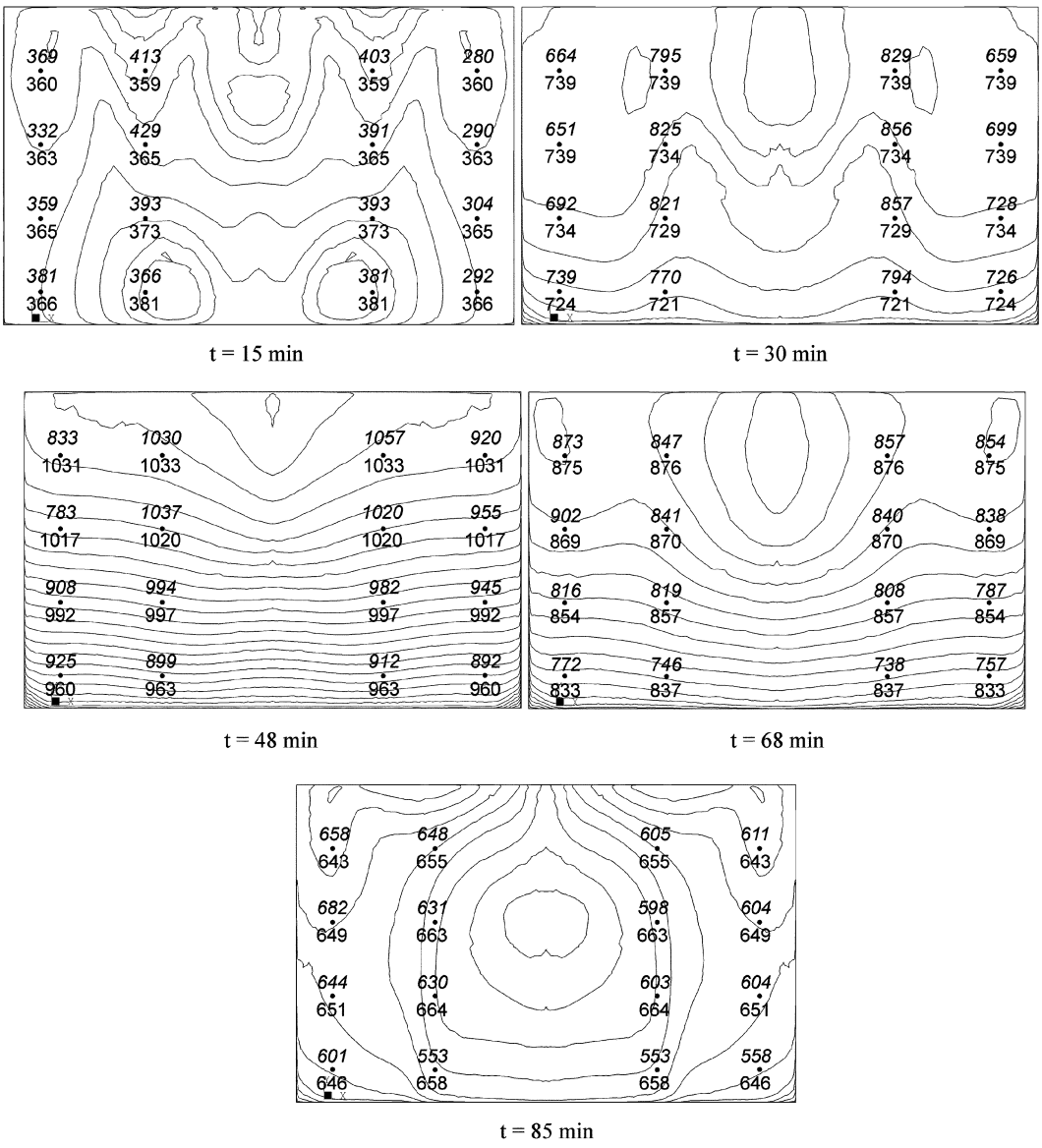

Fig. 12 Temperature distribution 300 mm below the compartment ceiling. Compartment opening is at the bottom.

observe that the agreement between numerical and experimental temperatures is, indeed, quite good, although during the very early stages of fire development, the numerical simulations slightly over-predict the gas temperature. There is also an over-prediction at the cooling phase, at the locations closer to the opening (Row-1). As anticipated, temperatures towards the compartment back (higher row index) are higher than temperatures near the opening. The parametric curve predicts a maximum average temperature of 1078ºC after 53 min and this compares well with the experimental results; however, this curve over-estimates the gas temperature during the early heating stage (Wald *et al.*

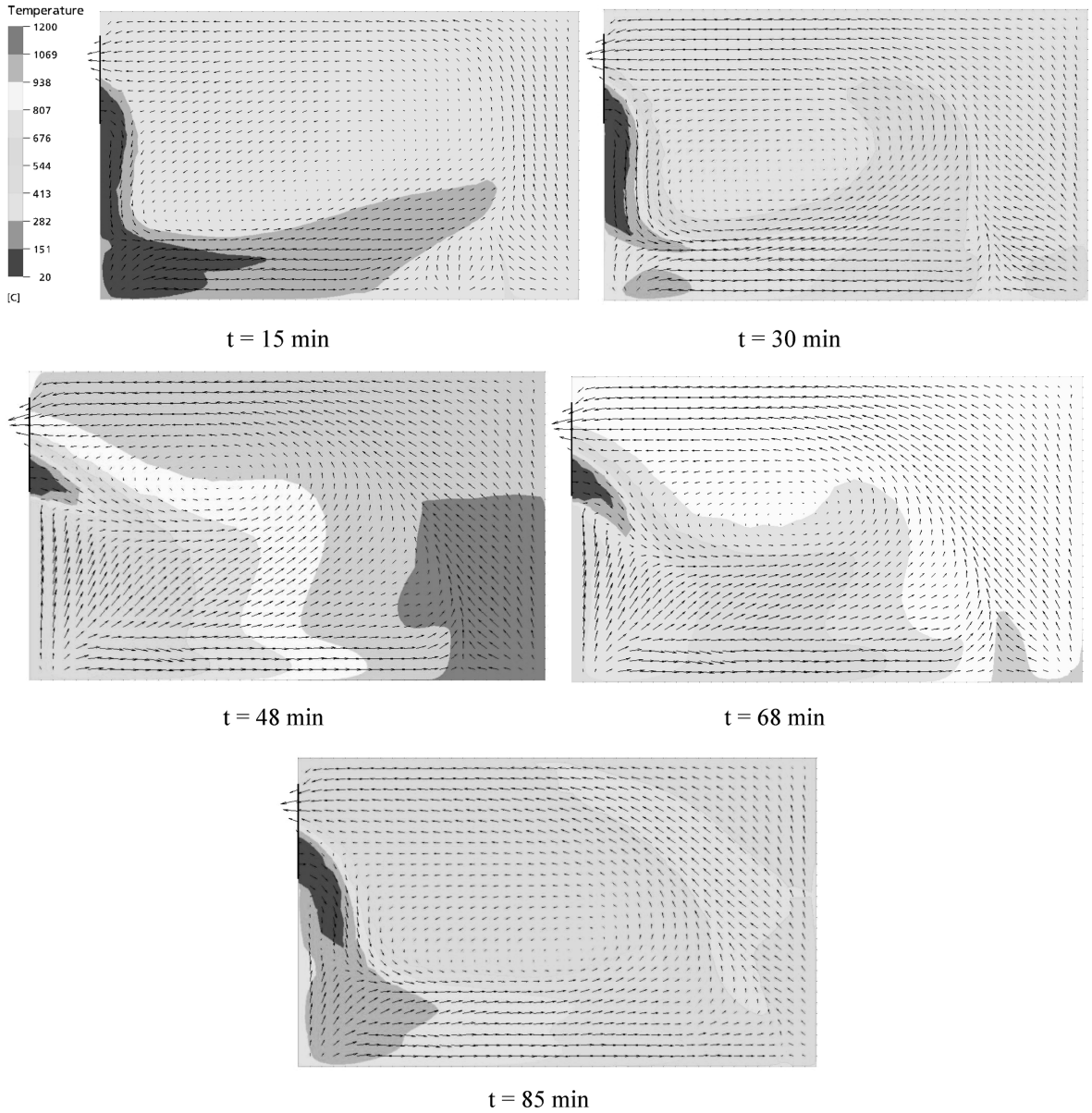

Fig. 13 Gas temperature distribution and velocity vector field at the compartment symmetry plane. Opening is at left.

2005). All the numerical results presented further on pertain RHR curve 2.

Temperature distribution at the vertical level of the experimental gas temperature measurements (300 mm below the ceiling) is shown in Fig. 12, for several time instants (as defined in Fig. 6). Here, we may observe the temperature contour levels for the numerical simulations, along with numerical and experimental temperature data at the marked punctual locations. Spacing between numerical temperature contours is 5°C. Figures near the dots are numerical results for temperature (below the dot) and corresponding thermocouple data (above the dot, in *italic*). We may observe that, in general, measured temperatures are lower at the right side of the compartment, while numerical data present, naturally, a

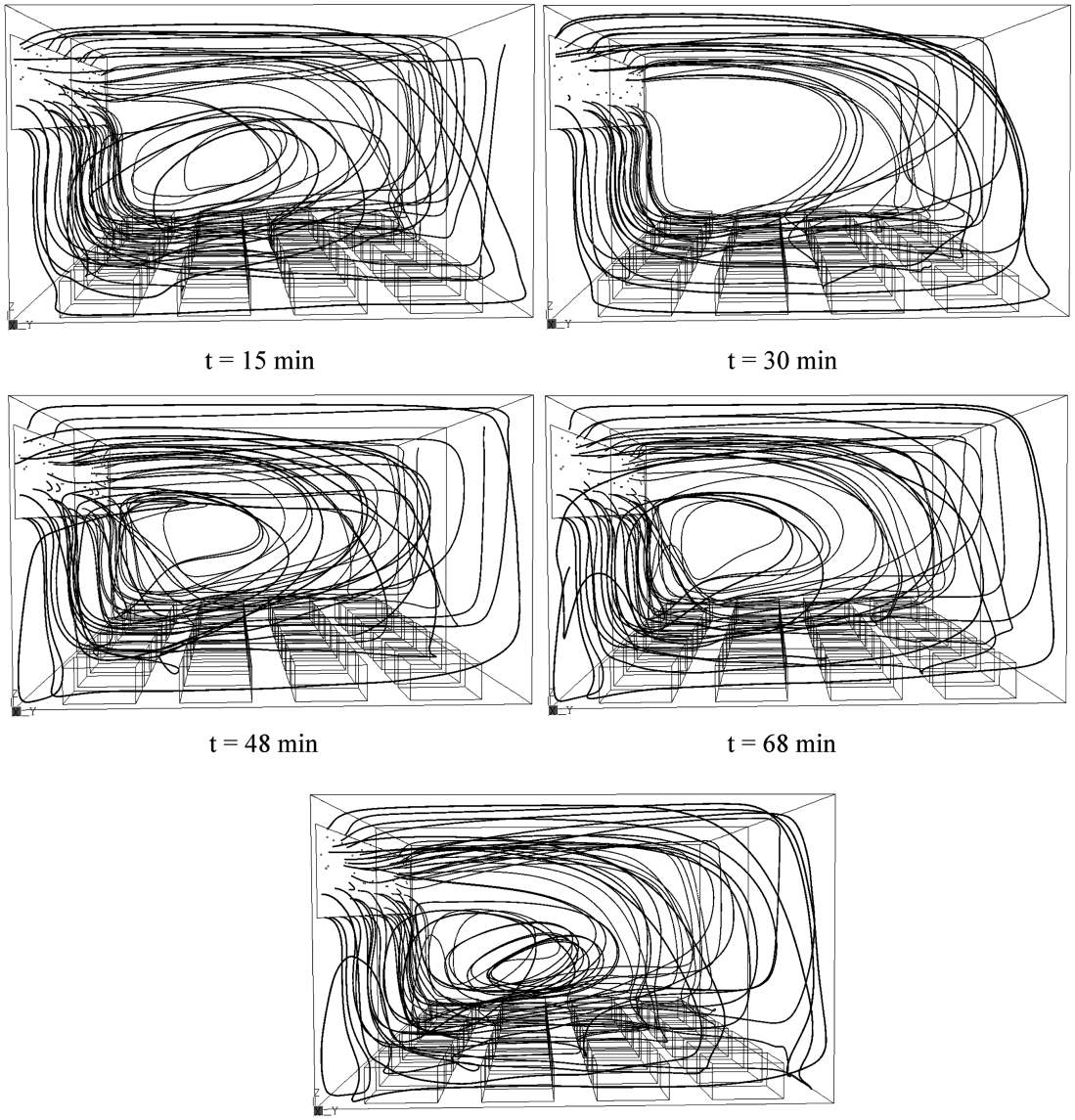

Fig. 14 Streamlines representation of the gas flow inside the compartment. Opening is at left.

perfect symmetry. At the very early stages, temperature within the compartment is quite uniform, with numerical data indicating slightly higher temperatures near the opening. This trend is not fully corresponded by the measurements, except for the left part of the compartment. As the overall flow circulation is established, a uniform pattern of increasing temperatures towards the compartment back takes place. Apart from some irregularity in the experimental data, the general agreement is quite satisfactory.

Numerical values for gas temperature at the compartment symmetry plane, together with the vector velocity field in a regular grid are represented in Fig. 13. It is important to note that, in order to improve the visualization of the velocity field pattern, the velocity vector scale is not the same in all the situations. These representations clearly show the cold air entrainment through the lower part of the opening, supplying the necessary oxygen for the combustion. This air mass is subsequently heated by the burning material, circulates inside the compartment, where it is cooled by the walls and then leaves through the upper part of the opening.

The gas flow pattern is best visualized using streamlines representation, as presented in Fig. 14. Apart from localized small flow patterns, the major noticeable feature is the large vortex that is formed within the confined space. It is interesting to note the absence of the convection column, typical of open-space fires. In fact, in this case, the height of the compartment is low when compared to the horizontal burning area and, consequently, due to the confinement, the gas flow is obliged to circulate according to the pattern depicted in these figures.

As the fire intensity increases, gas flow velocity will naturally increase as well. The gas flow velocity and temperature profiles through the vertical symmetry line of the opening are represented in Fig. 15, for the time instants considered previously. The hot gases leaving the compartment have a lower density than the cold air that is entering, thus explaining the higher velocities at the top-half of the compartment opening. The net air volume flow is thus, naturally, imbalanced. It is worth noting that the

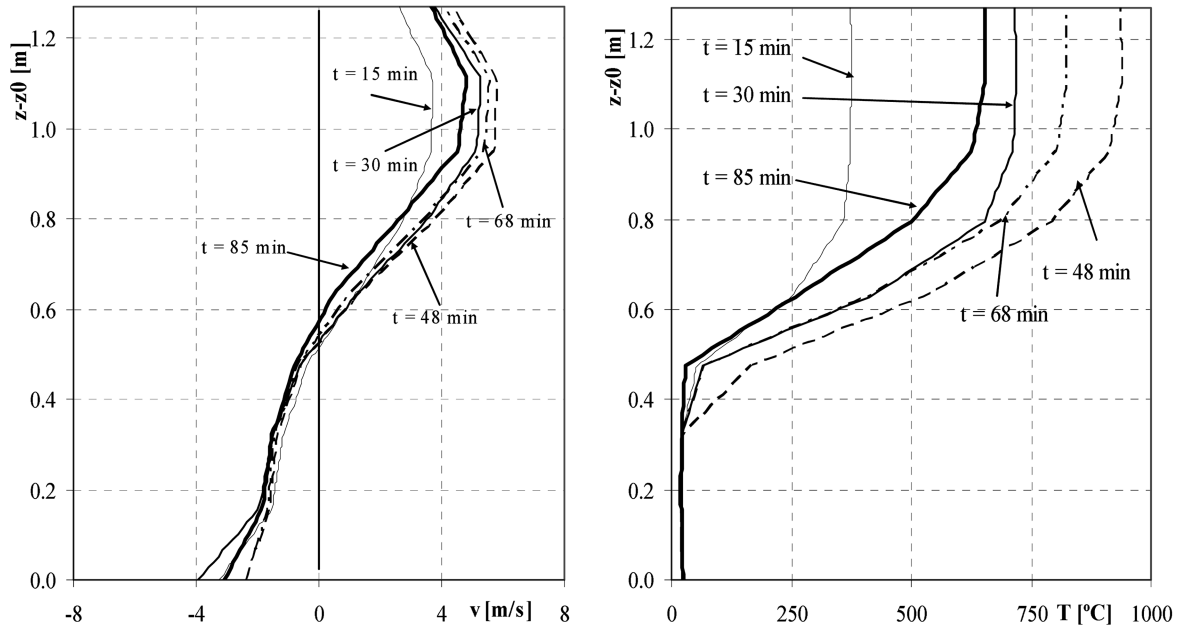

(a) – Vertical velocity profile (b) – Temperature vertical profile

Fig 15. Profiles through the vertical symmetry line of opening

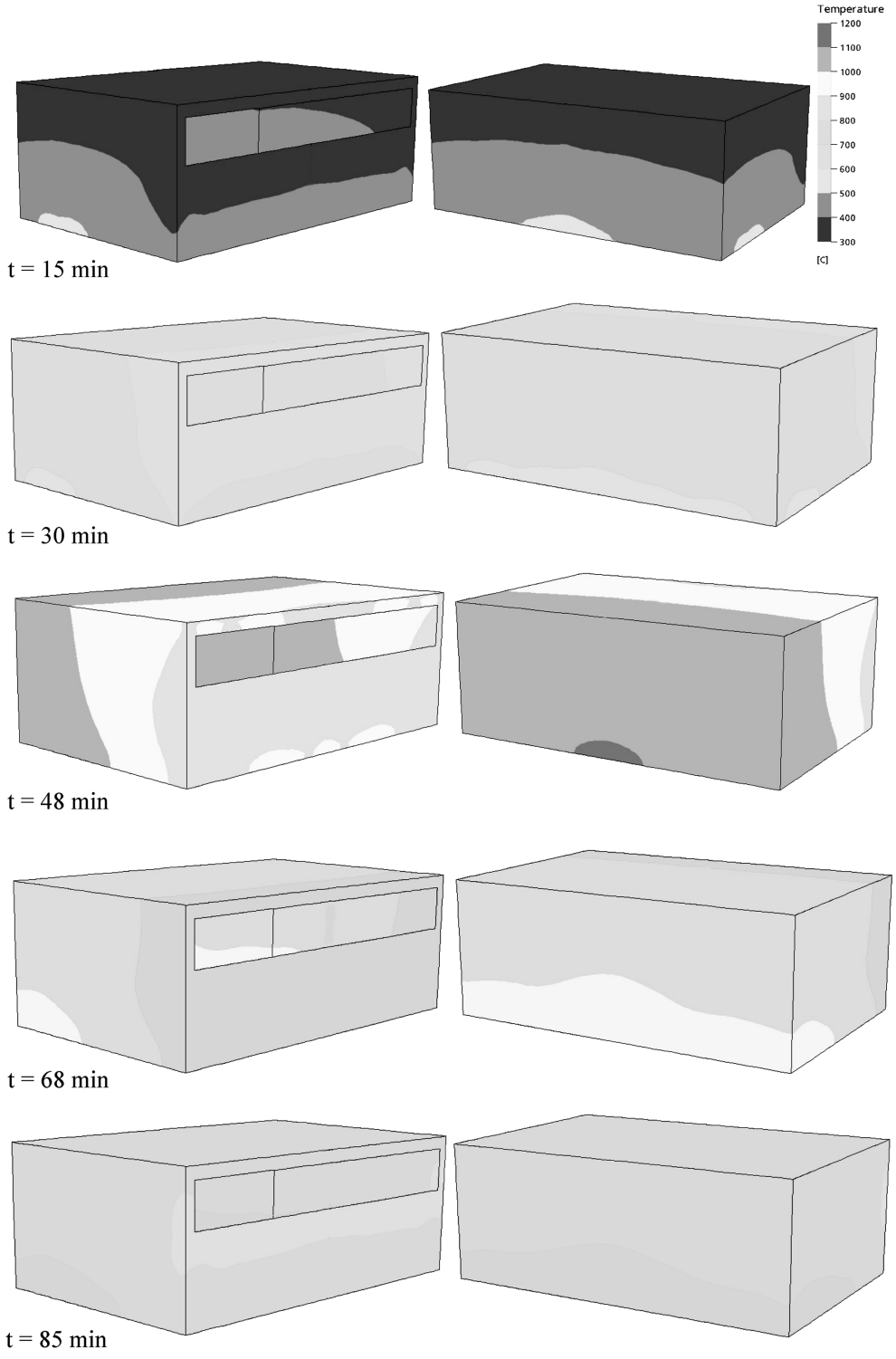

Fig. 16. Colour-shaded contours representing wall temperature

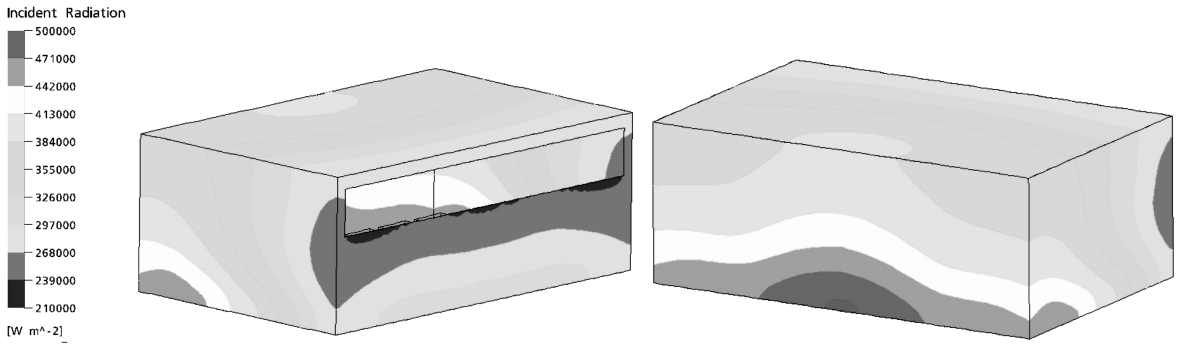

t = 68 min

Fig. 17 Colour-shaded contours representing radiative heat flux at the walls

amount of airflow through the opening affects to a great extent the development of the temperature field within the compartment. The temperature profiles show air at ambient temperature entering the domain and much hotter gases leaving. The leaving hot gases do not exceed 1000°C, though inside the compartment the maximum gas temperature is about 1160°C, near the heat sources.

Distribution of wall temperature is depicted in Fig. 16. The location of maximum gas temperature is at the bottom-back of the compartment, where the gas just passed over the heat source but is still not yet cooled by the colder walls. Maximum surface temperature is about 1110°C, at the bottom-back of the compartment.

Radiation received at a certain location in space is a complex conjugation resulting from the emissions from the surrounding surfaces, and gases as well. Radiation intensity distribution at the walls is represented in Fig. 17, for time instant t = 68 min. It may be noticed that the pattern obtained has some resemblance with the surface temperature pattern, as the local surface temperature is very much dependent on radiative heat transfer.

6. Conclusions

The present work showed that numerical simulation of a compartment fire, although computationally relatively expensive, is a good approach for providing detailed data on gas and surfaces temperature, heat fluxes and gas velocity field. A crucial point in the simulations is a physically realistic modelling of the rate of heat release as a function of time. Comparison of experimental, analytical and numerical data for punctual gas temperatures showed, for the present case, a quite good agreement.

The present fire experiment represents a quite rich and complex physical phenomenon. As such, its simulation is a challenging task, leaving many aspects for improvement. Perspectives for future work include: (1) study of the influence of the inclusion of production/destruction of turbulence kinetic energy due to thermal effects (Markatos *et al.* 1982, 1984); (2) modelling of the thermal inertia of the walls; (3) modelling the time evolution of the optical characteristics of the gas medium as a function of the burning conditions.

References

Bravery, P.N.R. (1993), "Cardington large building test facility - Construction details for the first building". England. Building Research Establishment, Internal paper, Watford.

Cadorin, J.F. and Franssen, J.M. (2003a), "A tool to design steel elements submitted to compartment fires-OZone V2. I. Pre- and post-flashover compartment fire model", *Fire Safety Journal*, **38**(5), 395-427.

Cadorin, J.F., Pintea, D., Dotreppe, J.C., Franssen, J.M. (2003b), "A tool to design steel elements submitted to compartment fires - OZone V2. II. Methodology and application", *Fire Safety Journal*, **38**(5), 429-451.

Cadorin, J.F. (2003), "Compartment fire models for structural engineering", Thése de Doctorat, Faculté des Sciences Appliqués, Université de Liège.

CFX-5.6 User's Manual, Ansys Incorporated.

Cox, G. (2001), "The capability of CFD fire simulation models", *Proc 9th Int. Fire Protection Symposium*, Vereinigung zur Forderung des Deutschen Brandschutzes, Braunschweig, 71-88.

Drysdale, D. (1999), *An Introduction to Fire Dynamics*, John Wiley & Sons, 2nd edn., New York.

Ewer, J., Galea, E.R., Patel, M.K, Taylor, S. and Knight, M. (1999), "An intelligent CFD based fire model", *J. of Fire Protection*, **10**(1), 13-27.

Harmathy, T.Z. (1978), "Mechanism of burning of fully-developed compartment fires", *Combustion and Flame*, **31**, 265-273.

Hoffmann, N. and Markatos, N.C. (1988), "Thermal radiation effects on fires in enclosures", *Appl. Math. Modelling*, **12**, 129-140.

Hoffmann, N., Galea, E.R. and Markatos, N.C. (1989), "Mathematical modeling of fire sprinkler systems", *Appl. Math. Modelling*, **13**, 298-306.

Launder, B.E. and Spalding, D.B. (1974), "The numerical computation of turbulent flows", *Comput. Methods Appl. Mech. Eng.*, **3**, 269-289.

Markatos, N.C, and Cox, G. (1984), "Hydrodynamics and heat transfer in enclosures containing a fire source", *PhysicoChemical Hydrodynamics*, **5**(1), 53-66.

Markatos, N.C, Malin, M.R. and Cox, G. (1982), "Mathematical modelling of buoyancy-induced smoke flow in enclosures", *Int. J. of Heat and Mass Transfer*, **25**(1), 63-75.

McGrattan, K.B, Baum, H.R., Rehm, R.G., Hamins, H. and Forney, G.P. (2000), *Fire Dynamics Simulator: Technical Reference Guide*, NISTIR 6467. Gaithersburg, MD: National Institute of Standards and Technology.

Menter, F.R. (1993), "Multiscale model for turbulent flows", *24th Fluid Dynamics Conf.*, American Institute of Aeronautics and Astronautics.

Menter, F.R. (1994), "Two-equation eddy viscosity turbulence models for engineering applications", *AIAA Journal*, **32**(8).

prEN 1991-1-2:2002: European Committee for Standardization (CEN). Eurocode 1: Actions on structures. Part 1.2: General actions – Actions on structures exposed to fire, Final Draft, April 2002, Brussels (2002).

Raithby, G.D. (1991), "Equations of motion for reacting, particle-laden flows", Progress Report, Thermal Science Ltd.

Rubini, P. (2000), *SOFIE (Simulations of Fires in Enclosures)*, School of Mechanical Engineering, Cranfield University, Cranfield, England.

Simões da Silva, L., Santiago, A., Vila Real, P. and Moore, D. (2005), "Behaviour of steel joints under fire loading", *Steel and Composite Structures*, **5**(6), 485-513.

Thomas, P.H. (1971), "Rates of spread of some wind driven fires", *J. of Forestry*, **44**(2), 155-175.

Vila Real, P. (2003), *Incêndio em Estruturas Metálicas*, Portugal, Edições Orion.

Wald, F., Simões da Silva, L., Moore, D., Lennon, T., Chladná, M., Santiago, A., Beneš, M. and Borges, L. (2005), "Experimental behaviour of steel structure under natural fire." *New Steel Construction*, **13**(3), 24-27.

Wald, F., Chladná, M., Moore, D., Santiago, A. and Lennon, T. (2004), "The temperature distribution in a full-scale steel framed building subject to a natural fire", *Proc. of the 2nd Int. Conf. of Steel and Composite Structures*, Seoul, Korea.

Wang, Y.C. (2002), *Steel and Composite Structures – Behaviour and Design for Fire Safety*, Spon Press, London.

Wilcox, D.C. (1993), "Turbulence Modeling for CFD", DCW Industries, Inc., La Canada, Califórnia, 460 p.

Annex A - prEN1991-1-2:2002 analytical curve

The evolution of gas temperature in the compartment during the heating phase is given by:

$$\theta_g = 1325(1 - 0.324e^{-0.2t^*} - 0.204e^{-1.7t^*} - 0.472e^{-19t^*}) \tag{A.1}$$

where t^* is a fictitious time (hours):

$$t^* = t\Gamma \tag{A.2}$$

and

$$\Gamma = \frac{(O/0.04)^2}{(b/1160)^2} \tag{A.3}$$

$$O = \frac{A_v\sqrt{h_v}}{A_t} \tag{A.4}$$

$$b = \sqrt{c\rho k} \tag{A.5}$$

where t is the time (hours) and c, ρ, k are the specific heat, density and thermal conductivity of compartment boundary, respectively.

The duration of the heating phase is determined by the fire load and the opening factor:

$$t_d^* = t_{\max}\Gamma \tag{A.6}$$

$$t_{\max} = \max\lfloor (0.2 \times 10^{-3} q_{t,d}/O);\ t_{lim} \rfloor \tag{A.7}$$

where $q_{t,d}$ is the design fire load density related to the total surface A_t:

$$q_{t,d} = q_{f,d}A_f/A_t \tag{A.8}$$

and $q_{t,f}$ is the design fire load density related to the floor surface A_f.

The time $t_{\max}$ corresponding to the maximum temperature is given by t_{lim}, if the fire is fuel controlled. If the fire is ventilation controlled, then $t_{\max}$ is given by the first term. When $t_{\max} = t_{lim}$, t^* used in equation (A.1) is replaced by:

$$t^* = t\Gamma_{lim} \tag{A.9}$$

$$\Gamma_{lim} = (O_{lim}/b)^2/(0.04/1160)^2 \tag{A.10}$$

$$O_{lim} = 0.1 \times 10^{-3} q_{t,d}/t_{lim} \tag{A.11}$$

If ($O > 0.04$ and $q_{t,d} < 75$ and $b < 1160$), Γ_{lim} has to be multiplied by k_t, given by:

$$k_t = 1 + \left(\frac{O - 0.04}{0.04}\right)\left(\frac{q_{t,d} - 75}{75}\right)\left(\frac{1160 - b}{1160}\right) \tag{A.12}$$

The temperature-time curve in the cooling phase is:

$$\begin{cases} \theta_g = \theta_{max} - 625(t^* - t^*_{max} x) & \text{for } t^*_{max} \le 0.5 \\ \theta_g = \theta_{max} - 250(3 - t^*_{max})(t^* - t^*_{max} x) & \text{for } 0.5 < t^*_{max} < 2.0 \\ \theta_g = \theta_{max} - 250(t^* - t^*_{max} x) & \text{for } t^*_{max} \ge 2.0 \end{cases} \tag{A.13}$$

where t^* is given the by equation (A.9), and:

$$t^*_{max} = 0.2 \times 10^{-3} q_{t,d} / O \tag{A.14}$$

$$\begin{cases} x = 1 & \text{for } t_{max} > t_{lim} \\ x = t_{lim} \Gamma / t^*_{max} & \text{for } t_{max} = t_{lim} \end{cases} \tag{A.15}$$

CC